ELECTRICAL CONTACT RESISTANCE MODEL FOR ALUMINUM RESISTANCE SPOT WELDING

M. PIOTT*, A. WERBER*, L. SCHLEUSS**, N. DOYNOV**, R. OSSENBRINK** and V. G. MICHAILOV**

*Daimler AG, Sindelfingen, Germany
**Department of Joining and Welding Technology, Brandenburg University of Technology, Cottbus-Senftenberg, Germany

DOI 10.3217/978-3-85125-615-4-36

ABSTRACT

Resistance spot welding is one of the most important welding processes for joining sheet metal parts in automotive industry. In the process of resistance spot welding electrical contact resistance is of critical importance. The process involves mechanical, electrical and thermal interactions and is dominated by Joule heating, generated at faying surfaces and electrode-sheet-interface. Especially for aluminum alloys, due to small bulk resistance and oxide layer, most of heat is generated at the interfaces.
Up to today, barely numerical models for the dynamic contact resistance of aluminum have been published. In this work, a model for contact resistance of aluminum alloys is presented. The model describes the dynamic contact resistance as a function of pressure and temperature.
Therefore, an experimental study was designed to determine the dynamic behavior of the contact resistance. Two sheets of aluminum alloy AA5182 were joined by resistance spot welding with variation of electrode force and current. In order to determine the apparent contact resistance, current and voltage differences between sheet-sheet and electrode-sheet were measured.
A coupled thermal-electrical-mechanical FE-model with temperature-dependent material properties was used to simulate the experiments. Calculated contact resistances and nugget diameters were compared to the measured ones in order to calibrate the contact resistance model and to validate the simulation.
Experimentally measured resistances and nugget diameters are in good accordance with numerical results. The dynamic contact resistance can be calculated by the deployed model with reasonable accuracy.

INTRODUCTION

Today, resistance spot welding (RSW) is one of the most frequently used joining processes in the body in white shop due to high ability for automation, low cost and short cycle time [1–3]. The required heat of the welding process is generated by Joule heating. The RSW process can be structured in the four process steps displayed in Fig. 1. First, a force is applied on the electrodes and two or more metal sheets are pressed together. In the second step, an electric current through the workpieces is applied and heat is generated by Joule heating, dependent on the distribution of bulk and contact resistances. With increasing temperature, material is softening and a molten nugget forms, when the temperature of the

faying surface reaches the melting point of material. After switching off current, the nugget solidifies under pressure and joins the sheets together. In the last step, electrode force is released and the electrodes are removed.

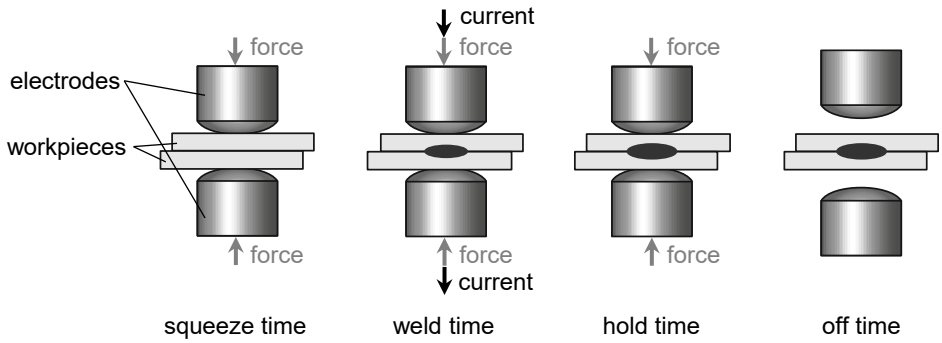

Fig. 1 Process steps of resistance spot welding

In order to save weight and reduce emissions, more light metal alloys, especially aluminum alloys, are utilized in the automotive industry [4, 5]. With the growing demand of aluminum, the need for integration of aluminum resistance spot welding increases. The welding behavior of aluminum is different from steel, which is already well integrated in the body in white shop. Higher currents and shorter process times are required for RSW of aluminum, due to higher electrical and thermal conductivity [6]. Furthermore, the rapidly forming oxide layer of aluminum significantly increases contact resistance and heat generation, which causes rapid electrode cap degradation [2]. Prerequisite of an extended integration of RSW of aluminum alloys into the body in white shop is an improved understanding of influencing parameters and inter-dependencies. Thereby process parameters and the machine setup can be optimized.

Fig. 2 shows the two kinds of resistances in RSW: contact and bulk resistance. The contact resistance appears at electrode-sheet and sheet-sheet interfaces (R_2, R_4 and R_6) and the bulk resistances in workpieces (R_3 and R_5) and electrodes (R_1 and R_7) [7].

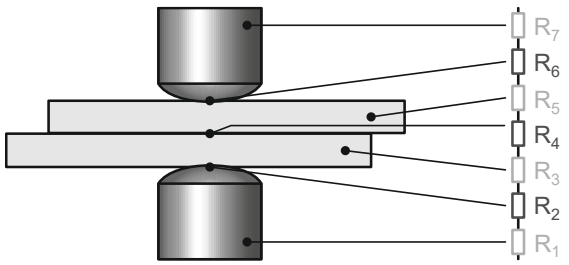

Fig. 2 Electrical resistances in resistance spot welding

The bulk resistance of aluminum alloys and copper increases with temperature. Due to low bulk resistances of aluminum and copper, RSW process of aluminum alloys is strongly influenced by contact resistances, depending on pressure, temperature and surface conditions of the interfaces. Additionally, aluminum alloys form an oxide layer, which is significantly increasing contact resistance. For a robust process, an uniform oxide layer is important. Therefore, aluminum suppliers use special surface treatments to create stable

and uniform oxide layers. Further conditions influencing the contact resistance are surface roughness, lubricants, contaminants and adhesives.

There are many different models for contact resistance in literature. Basics of electrical contacts were studied by Holm [8]. There, it was assumed, that the real contact area is only part of the apparent contact area due to surface roughness. As a result, Holm divided the contact resistance into constriction and film resistance. The constriction resistance represents the constriction of current flow due to surface roughness, see Fig. 3. Thus, the conducting real contact area is always smaller than the apparent contact area. According to Holm, the constriction resistance R_c depends on the bulk resistivity ρ_{el} and the radius of a circular contact spot a:

$$R_c = \frac{\rho_{el}}{2a} \tag{1}$$

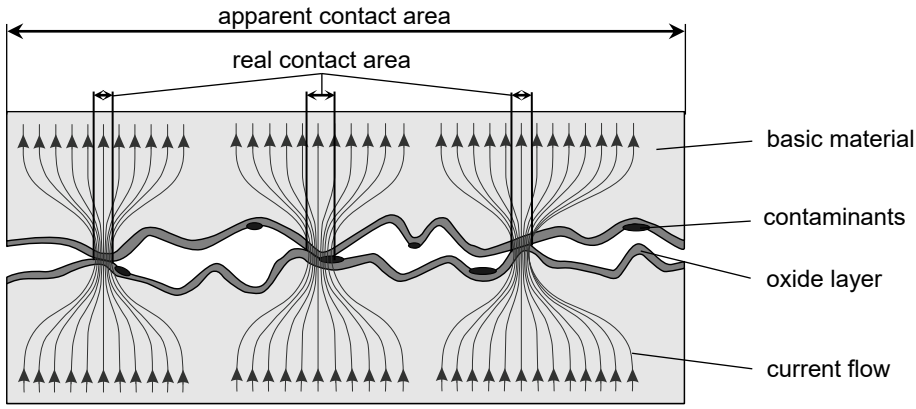

Fig. 3 Surface morphology of electrical contact of aluminum surfaces based on [9]

Metallic surfaces are generally contaminated with an insulating or poorly conducting film layer or residues of lubricant, which influence the conducting contact area and increase contact resistance [10]. Especially aluminum alloys exhibit a rapidly forming oxide layer that is highly increasing contact resistance as film resistance [2].

By generation of heat due to Joule heating in RSW process, contact surface is changing. Increasing temperature of contact asperities result in a thermal expansion, which leads to film rupturing. High loads and high currents can yield to further ruptures of the film. Real contact area increases with growing temperatures due to material softening. Additionally, bulk resistance of contacting materials is increasing with temperature. These effects are superimposed and dynamic. Thus, separating bulk and contact resistance in experiments is not possible.

There are different possibilities to characterize the temperature and pressure dependent behavior of the contact resistance. In situ measurements determine the dynamic behavior of the absolute resistance during RSW-process. Thus, separating bulk and contact resistance in in situ measurements is not possible, because the temperature and pressure distribution in the contact interface is unknown and very dynamic. Therefore, numerical simulation can be used to determine contact resistance inversely [11, 12]. In ex situ measurements the geometry and the conditions of contact interface are simplified in order to control temperature and pressure of contact interface [13–16]. Thus, the specific contact resistance

can be determined, but this method cannot reproduce the dynamically changing contact area and contact conditions during RSW-processes.

In literature, several analytical models of contact resistance have been published. Holm presented a formula for clean contacts based on contact load and material hardness [8]. Other researchers suggested models, which describe the constriction resistance dependent on surface roughness, like Greenwood and Williamson [17, 18]. These models usually rely on surface parameters, which are difficult to determine. Zhang describes contact resistance as a function of flow stress, pressure, bulk resistivity of materials and film resistivity [19]. Popov presented a model for clean contacts, which depends on material bulk resistivity and surface
roughness [20]. Kaars published a simple contact resistance model for aluminized steel, where contact resistance is a combination of pressure and temperature dependent functions [12].

In summary, several models for contact resistance are published, but they are usually limited to clean contact faces or rely on parameters, which are difficult to determine. Further, many models describe the behavior of contact resistance for steel and cannot be directly transferred to aluminum alloys.

The current investigation focuses on RSW of aluminum alloy AA5182, which is well integrated in the body in white shop. A model for dynamic contact resistance, depending on contact pressure and temperature, is presented. It considers coupled thermal-electrical-mechanical FE-formulation. To calibrate the model, experiments were carried out, joining two sheets by RSW with variation of electrode force and current. A direct measurement of contact resistances in experiments is not possible. Thus, coupled thermal-electrical-mechanical FE-simulations are carried out to analyze the RSW process. By measuring current and voltage differences between sheets as well as electrode and sheet, the apparent contact resistances, which contain contact and bulk resistances, can be evaluated. FE-simulations with temperature-dependent properties are performed to develop and calibrate a contact resistance model by simulation of the experiments. The FE-model gets validated by comparison of experimental and simulated nugget dimensions.

EXPERIMENTAL SETUP

The experimental setup is developed to determine resistance curves and to calibrate the model for electrical contact resistance with numerical simulations. Therefore, welding experiments are carried out with two samples of aluminum sheets with same thickness in each case. The dimensions of the sheets are 80 mm × 50 mm with a thickness of 0.85 mm and 1.5 mm, respectively. Sheet material is aluminum alloy AA5182 with a Ti-Zr based conversion layer and lubricant. These workpieces are joined with electrode caps of type ISO 5821-A0-16-20-100 and material CuCr1Zr (ISO 5182-A2/2) by one single spot, Fig. 4.

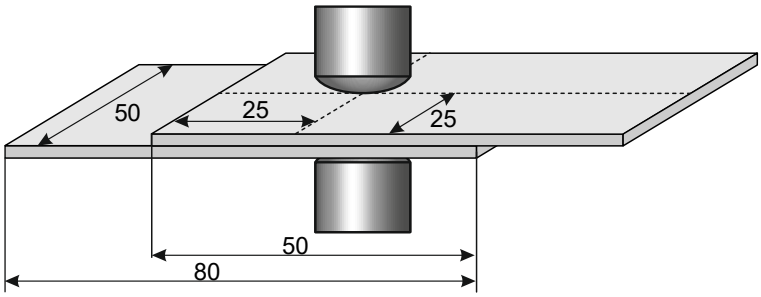

Fig. 4 Experimental setup

The applied welding current was DC, delivered by an inverter power source clocked with 1 kHz. Two different welding current programs were applied. First current program uses a preheating current of 8 kA and a slope up to the main welding current of 27 kA. The second program has a slope of 50 ms with increasing current from zero to 25 kA. Afterwards, the current is constant for 100 ms. In both programs, electrode force is set constant to 3 kN, 4 kN or 5 kN. Electrode force was applied pneumatically. For each force and current program, five experiments were performed. The electrode forces and current programs are visualized in Fig. 5 and parameter sets are summarized in Table 1.

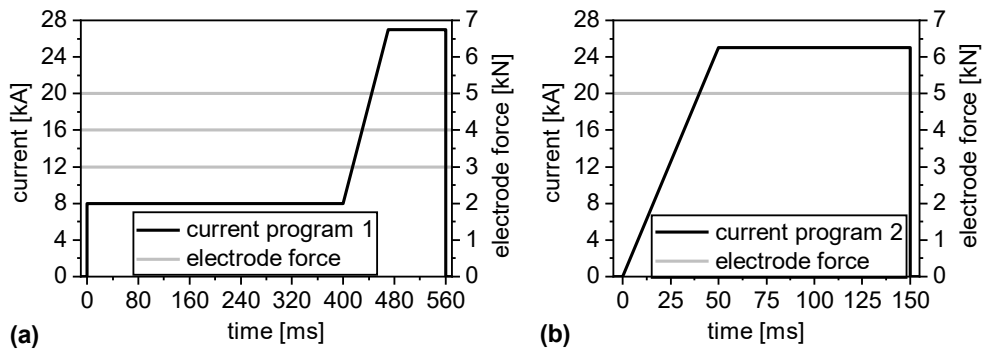

Fig. 5 Process conditions for experiments: (a) electrode forces with current program 1 and (b) electrode force with current program 2

Table 1 Sets of parameters in experiments

Set	Sheet thickness [mm]	Current program	Preheating current [kA]	Main current [kA]	Electrode force [kN]
1	0.85	1	8	27	5
2	0.85	1	8	27	4
3	0.85	1	8	27	3
4	0.85	2	-	25	5
5	1.5	1	8	27	5

In order to determine electrical resistances during RSW, the electrical voltage differences between lower electrode and lower sheet, upper sheet and upper electrode were measured. Voltages at sheets were tapped with clamps and a copper wire was soldered onto each

electrode. Additionally the voltage difference between the electrodes was measured twice for verification of measurement. Furthermore, the current flow was measured by a Rogowski coil and electrode force was measured by strain gauges, which have been calibrated before. Fig. 6 shows the experimental setup. The experimental resistances between sheet-sheet (R_2') and between electrode-sheet (R_1' and R_3') can be determined by equ. (2).

$$R' = \frac{\Delta U}{I} \tag{2}$$

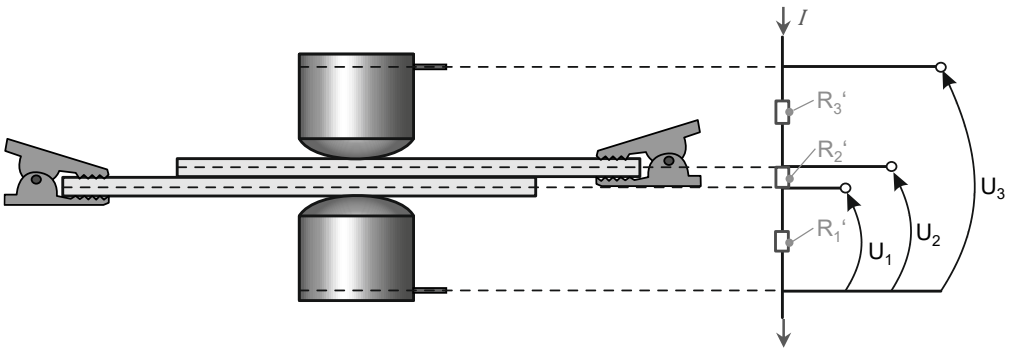

Fig. 6 Measurement of potentials and resistances

FINITE ELEMENT MODEL FOR ALUMINUM SPOT WELDING

RSW is a complex process with interactions of mechanical, electrical and thermal phenomena. So a coupled thermal-electrical-mechanical FE-model is set up to consider the essential effects of the welding process. For the numerical simulation, the problem formulation is separated in three sequentially coupled fields: a mechanical, a thermal and an electrical. This chapter gives a short introduction into the used FE-model.

A simplified model is used for FE-simulations, with respect to axial symmetry. Fig. 7 shows the geometry with initial and boundary conditions. The magnitude of initial and boundary conditions of the FE-model are summarized in Table 2.

Table 2 Initial and boundary conditions of FE-simulation

Parameter	Unit	Magnitude
Initial electrode temperature $T_{0,E}$	°C	20
Initial sheet temperature $T_{0,S}$	°C	25
Cooling water temperature T_W	°C	20
Ambient temperature T_{Amb}	°C	25
Convective heat transfer coefficient α_A	W/(m² K)	25

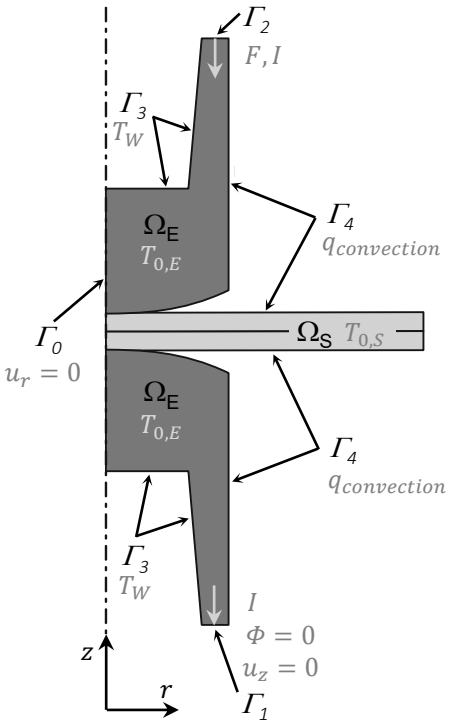

Fig. 7 Initial and boundary conditions

By neglecting inductive effects, the static electrical field is characterized by Ohm's law according to:

$$\mathrm{J} = \frac{1}{\rho_{\mathrm{el}}}\mathrm{E} = -\frac{1}{\rho_{\mathrm{el}}}\nabla\Phi \tag{3}$$

where J denotes the current density, E designates the electrical field, ρ_{el} is the electrical bulk resistivity of material and Φ is the electrical potential. The electrical potential on surface Γ_1 is zero as shown in equ. (4) and the electrical current through surfaces Γ_1 and Γ_2 is defined by the applied welding current I, which is directed towards y-axis. The other surfaces are considered to be insulating.

$$\Phi = 0 \quad (\text{boundary } \Gamma_1) \tag{4}$$

Heat generation in RSW is dominated by Joule heating, which is caused by current flow. The increase of temperature yields to a heat conduction problem. The transient heat conduction is described by linear Fourier's law with internal heat source as heat generations per unit volume. The Joule heating per unit volume q_J depends on resistivity of material ρ_{el} and current density J according to equ. (5). The effect of liquid flow in the molten nugget is neglected, due to small size of nugget weld pool and short welding time [21].

$$\mathrm{q_J} = \rho_{\mathrm{el}}\,\mathrm{J}^2 \tag{5}$$

The thermal initial conditions for electrodes and sheets (Ω_E and Ω_S) are equal to initial temperature T_0, as shown in equ. (6). The thermal boundary condition on surface Γ_3 is defined equal to the temperature of the cooling water T_W (equ. (7)) and a convective heat flux rate $q_{convection}$ is applied at surface Γ_4 according to equ. (8), where α_A denotes the convective heat transfer coefficient, T is the surface temperature and T_{Amb} is the ambient temperature. The other surfaces are considered adiabatic.

$$T_{initial} = T_0 \quad (\text{domain } \Omega_E \text{ and } \Omega_S) \tag{6}$$

$$T = T_W \quad (\text{boundary } \Gamma_3) \tag{7}$$

$$q_{convection} = \alpha_A (T - T_{Amb}) \quad (\text{boundary } \Gamma_4) \tag{8}$$

The mechanical problem considers small deformations. The material behavior is described by constitutive linear momentum balance equation, relating the stress to imposed strain due to electrode force and thermal strain. The thermal strain results from calculated transient temperature field, considering linear isotropic expansion coefficient. The electrode force F is applied as a set of traction boundary condition at boundary Γ_2. A displacement boundary condition is defined on all points of boundary Γ_1, where the displacement component u_z is set to zero:

$$uz\ u_z = 0 \quad (\text{boundary } \Gamma_1) \tag{9}$$

The displacement boundary condition u_r results from axial symmetry and is applied on all nodes of Γ_0:

$$uru_r = 0 \quad (\text{boundary } \Gamma_0) \tag{10}$$

In the FE-model of RSW, the electrodes are modeled elastic and sheets are defined elastoplastic with isotropic hardening using the von Mises yield criterion. The governing equation for elastic behavior in incremental form is shown in equ. (11). $\{d\sigma\}$ denotes the stress increment, $\{d\varepsilon^e\}$ is the elastic strain increment and $[D]$ is the elastic matrix.

$$\{d\sigma\} = [D]\{d\varepsilon^e\} \tag{11}$$

Plastic deformation starts, when the von Mises equivalent stress $\bar{\sigma}$ reaches the flow stress of the elastoplastic material σ_F, according to equ. (12). The associated plastic strain can be calculated by equ. (13) and equ. (14). $\boldsymbol{S}$ denotes the deviatoric stress tensor, $\dot{\boldsymbol{\varepsilon}}^p$ is the plastic strain rate and $\dot{\bar{\varepsilon}}^p$ is the equivalent plastic strain rate.

$$\bar{\sigma} = \sqrt{\frac{3}{2}\boldsymbol{S}^T\,\boldsymbol{S}} \leq \sigma_F \tag{12}$$

$$\dot{\bar{\varepsilon}}^p = \sqrt{\frac{2}{3}\dot{\boldsymbol{\varepsilon}}^{pT}\dot{\boldsymbol{\varepsilon}}^p} \tag{13}$$

$$\dot{\boldsymbol{\varepsilon}}^p = \frac{3}{2}\frac{\dot{\bar{\varepsilon}}^p}{\bar{\sigma}}\boldsymbol{S} \tag{14}$$

Material properties of the elastoplastic material model are defined as nonlinear functions of temperature up to melting temperature, like presented in [22]. Electrical resistivity, thermal properties, density and flow curves of AA5182 are based on experiments ranging from room temperature to 500 °C. Thermal data above 500 °C is extrapolated and Young's modulus as well as Poisson's ratio are based on data generated by software JMatPro®. Furthermore, phase change is taken into account by latent heat. The material properties of AA5182 at room temperature are shown in Table 3.

Table 3 Material properties of aluminum alloy AA5182 at room temperature

Yield Stress	Young's Modulus	Poisson's Ratio	Density	Electrical Resistivity	Specific Heat	Thermal Conductivity	Thermal Expansion
MPa	MPa	-	g/cm³	µΩ m	J/(kg K)	W/(m K)	-
155	70000	0.33	2.62	0.06	926	110	$24 \cdot 10^{-6}$

In order to simulate RSW, a model of the dynamic behavior of contact resistance at faying interface and electrode-sheet interface is required. In the following, an approach for contact resistance, considering the elementary effects of RSW, is described.

The dynamic absolute contact resistance R is connected to specific contact resistance $r(p,T)$ and apparent contact area A according to equ. (15).

$$R{=}rp{,}TA\ R = \frac{r(p,T)}{A} \tag{15}$$

Assuming that the specific contact resistance is a function of pressure and temperature. Effects of pressure and temperature are assumed to be independent. Effects of time are neglected. Thus, the contact resistance $r(p,T)$ can be described as:

$$rp{,}T{=}r0\ fT\ r(p,T) = r_0 f(T) g(p) \tag{16}$$

where r_0 is a basic contact resistance, $f(T)$ and $g(p)$ are functions of temperature and pressure, respectively. The basic contact resistance depends on the interface (electrode-sheet or sheet-sheet), the conducted materials and surface morphology (passivation, oxide layer, lubricant, surface roughness and contaminants).

Based on literature [8, 19, 12, 16], the function of pressure is defined as:

$$g(p) = \left(\frac{p_k}{p + p_k}\right)^n \tag{17}$$

wherein p is the contact pressure and p_k is a constant to avoid numerical instabilities for a contact pressure equal to zero. The pressure exponent n gets determined by simulations.

In many contact resistance models, the temperature dependency of contact resistance is considered by hardness or flow stress of materials. To obtain a more universal model, the

temperature function is defined by a nonlinear curve, which gets investigated iteratively by simulations.

RESULTS AND DISCUSSION

The measured current and electrode forces have little difference compared to the machine settings (Fig. 5). Fig. 8 shows examples of measured data for current program 1. Electrode force shows small increase at current slope due to high thermal expansion, which can not be compensated by the control of the welding gun. Further, the measured current has some differences due to the current control of the welding gun. In order to include these effects in FE-simulation, measured current curves and electrode forces are used in simulation. Experiments with splashes are excluded from evaluation.

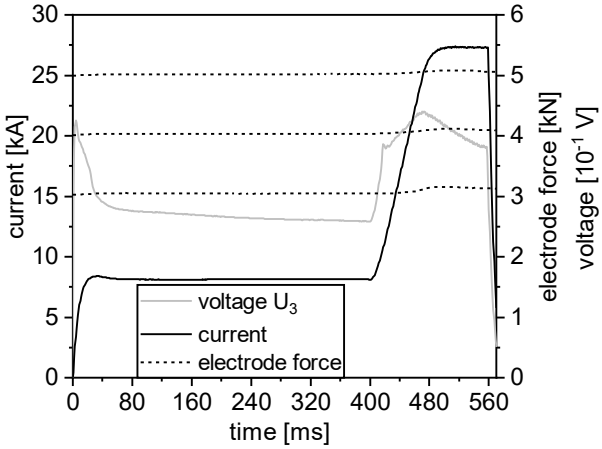

Fig. 8 Examples of measured current, voltage and electrode force at current program 1

CALIBRATION OF CONTACT RESISTANCE MODEL

In order to calibrate the contact resistance model, measured curves of apparent contact resistances for sheet-sheet and electrode-sheet are used. Resistances are determined by the recorded voltage differences and currents. All measured apparent contact resistance curves have the maximum resistance at the beginning, due to the smallest real contact area and lowest temperature, visualized in Fig. 9 and Fig. 10 The contact resistance is rapidly decreasing due to an increasing amount and deformation of asperities with temperature, which are influencing the contact constriction resistance [10]. Regarding contact resistance, there is a difference in the behavior of current program 1 and current program 2. The preheating current of program 1 yields to a nearly constant resistance, see Fig. 9. With increasing current up to the main welding current, the resistance is falling to a minimum. In contrast, the measured resistance of current program 2 in Fig. 10 is steadily decreasing to an almost constant level. The comparison of simulated and measured results shows a qualitative good accuracy. Up to 25 ms process time, the simulated resistance is smaller

than the measured ones. This error is assumed to be tolerable, because current and generated Joule heating is small.

For calibration of contact resistance model, parameters of presented contact resistance model are optimized by numerical simulations to fit of measured curves. First, boundary conditions of temperature function are defined. The value of temperature function at room temperature was set to one and the value of zero was applied at melting temperature of aluminum. Values of steadily decreasing temperature function between room temperature and melting temperature, parameters r_0 and n of equ. (16) and equ. (17) are determined by simulation.

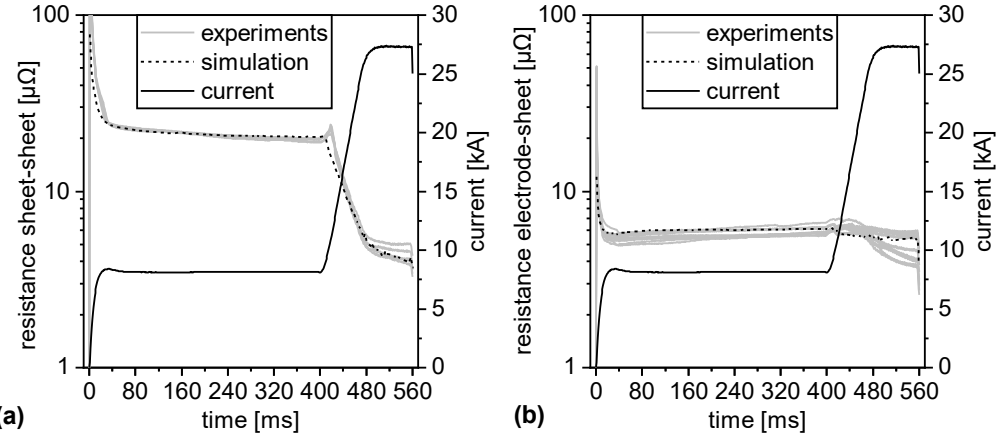

Fig. 9 Experimental apparent contact resistance curves between (a) sheet-sheet and (b) electrode-sheet with electrode force 5 kN, current program 1 and sheet thickness 0.85 mm

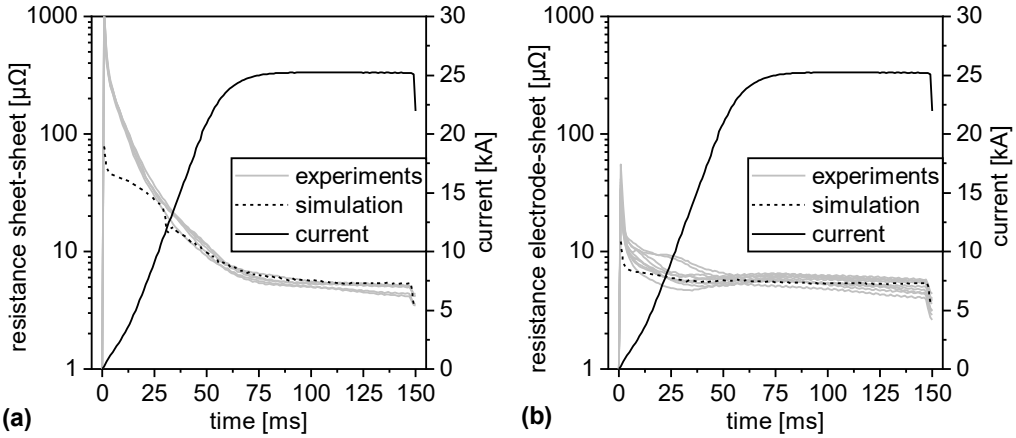

Fig. 10 Experimental apparent contact resistance curves between (a) sheet-sheet and (b) electrode-sheet with electrode force 5 kN, current program 2 and sheet thickness 0.85 mm

The results of simulative calibration of the dynamic contact resistance model for AA5182 are shown in Fig. 11. Further parameters of the model are summarized in Table 4. Thus, pressure exponent n is determined to be 1/3 and the corrective term is set to 0.001 GPa, considering pressure p in GPa. The temperature dependent function is

decreasing from one at room temperature to zero at melting temperature. Further, a drop of temperature function can be seen between 400 °C and 450 °C. The basic contact resistance of electrode-sheet interface is much smaller than basic resistance of sheet-sheet interface, see Table 4. Reason for this effect could be the rupturing of aluminum oxide layer at electrode-sheet interface due to electrode hardness, high electrode forces and electrode radius. In all presented results of FE-simulations, the described dynamic contact resistance model is used.

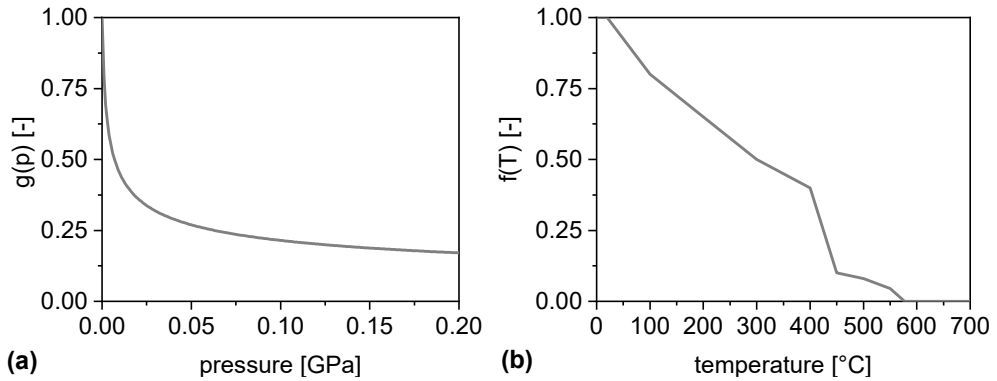

Fig. 11 Functions of the contact resistance model: (a) pressure and (b) temperature

Table 4 Parameter of contact resistance model for the sheets with thickness 0.85 mm

Parameter	Unit	Magnitude
r_0 (electrode-sheet)	μΩ mm²	50
r_0 (sheet-sheet)	μΩ mm²	3 650
n	-	1/3
p_k	GPa	0.001

In experiment, only the apparent contact resistance can be measured. By recording voltages and currents, measured resistances are always a combination of contact resistance and bulk resistances of materials between the taps. In contrast, FE-simulation enables the determination of real contact resistance. Fig. 12 visualizes the calculated contact resistance. Further, bulk resistance, which depends on material bulk resistivity and the conducted are, is shown. Up to the slope time, the apparent resistance at the faying surface is dominated by contact resistance for current program 1. Afterwards, the contact resistance is breaking down, due to melting process. At electrode-sheet interface, the apparent contact resistance is dominated by bulk resistance.

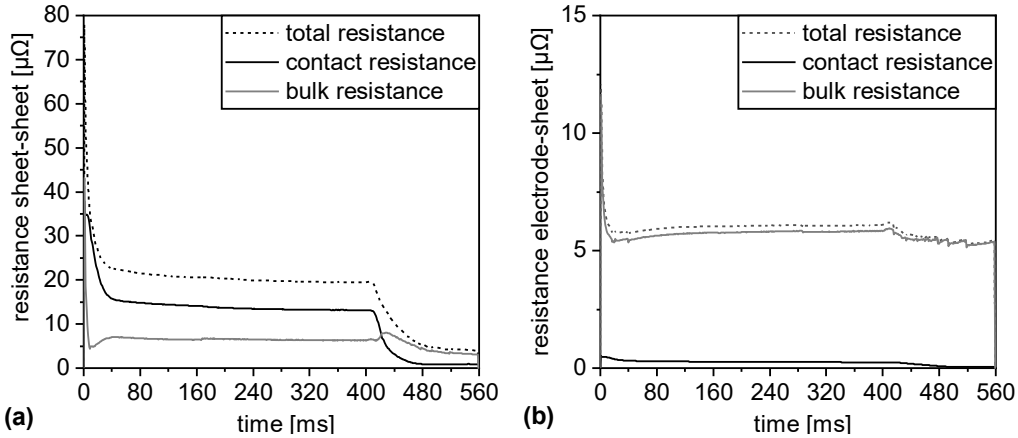

Fig. 12 Calculated total, contact and bulk resistances with electrode force 5 kN, current program 1 and sheet thickness 0.85 mm for (a) sheet-sheet interface and (b) electrode-sheet interface

Heat generation due to Joule heating is shown in Fig. 13 for current program 1, electrode force of 5 kN and sheet thickness 0.85 mm. Most heat (about 1080 J in experiments and 1043 J in simulation) is generated at sheet-sheet interface caused by contact and bulk resistances. In contrast, Joule heating at electrode-sheet (about 586 J in experiment and 617 J in simulation) is smaller for electrode force of 5 kN. Generated heat caused by contact resistance is about 534 J at faying interface and Joule heating due to contact resistance at electrode-sheet interface is essentially smaller (about 14 J).

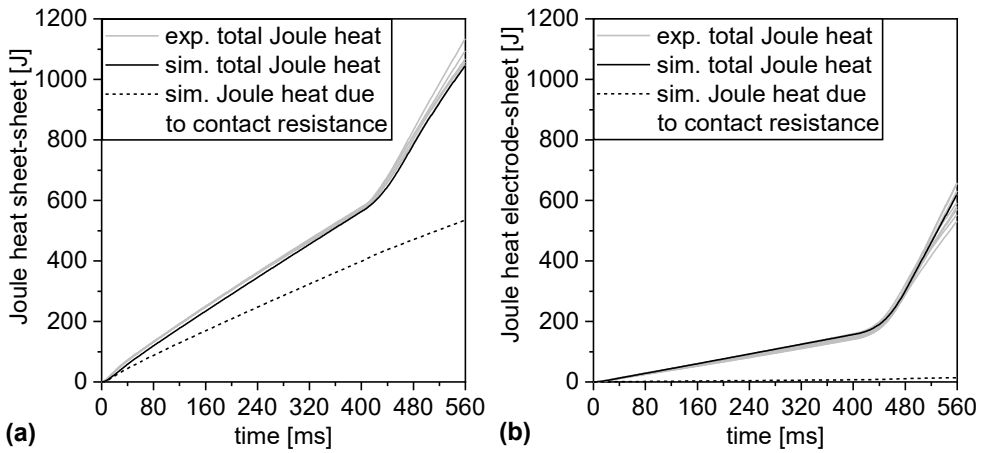

Fig. 13 Measured and simulated Joule heat with electrode force 5 kN, current program 1 and sheet thickness 0.85 mm for (a) sheet-sheet interface and (b) electrode-sheet interface

In order to determine the deviation between measured and simulated results, total heat generated by Joule heating at faying interface and electrode-sheet interface are compared in Fig. 14 and Fig. 15, respectively. The resulting averaged deviation for generated Joule heating between calculated and mean measured heat is about 3% for faying interface and

about 5% for electrode-sheet interface. Thus, the results of FE-simulation are matching experiments with a high accuracy.

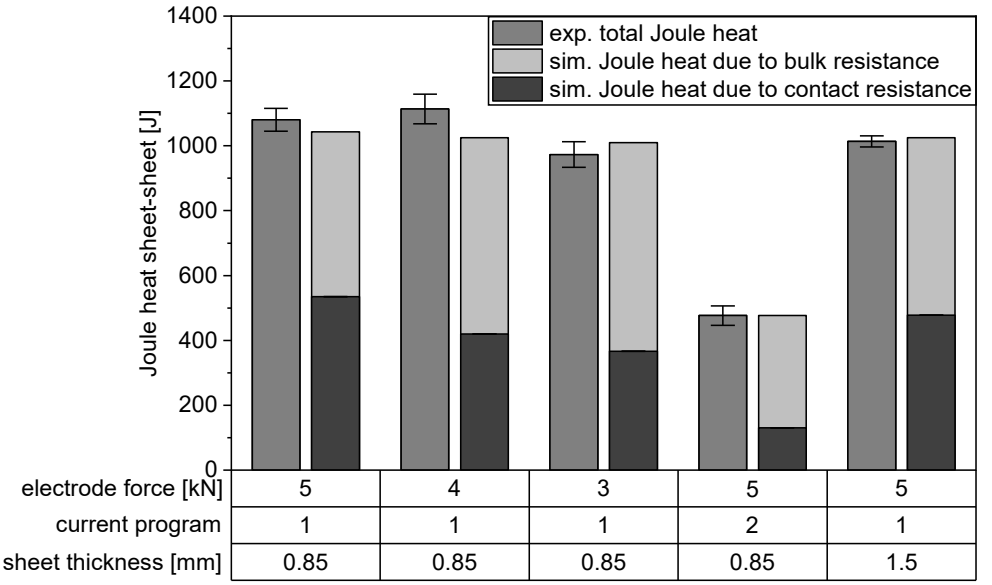

Fig. 14 Measured und calculated Joule heat at faying interface

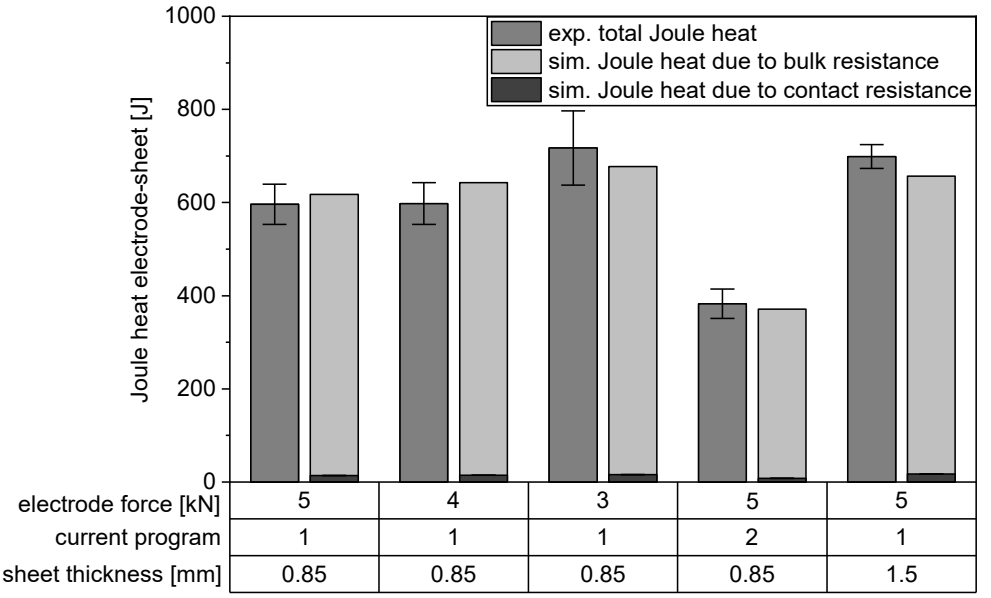

Fig. 15 Measured und calculated Joule heat at electrode-sheet interface

VALIDATION OF FE-MODEL

For validation of the developed FE-model and the contact resistance model, calculated and measured nugget dimensions are compared in Fig. 16. Therein, measured weld diameters are compared to simulated nugget diameters due to asymmetric nuggets. By decreasing electrode force from 5 kN to 3 kN, mean weld diameter is growing from 4.0 mm to 6.5 mm for sheet thickness 0.85 mm. Mean weld diameter of 4.5 mm at current program 2 is greater than the one of current program 1, although the main current is 2 kA less. The increasing sheet thickness to 1.5 mm yields to bigger nuggets. In experiments the weld diameter grows to 5.0 mm. With a mean discrepancy of about 4% between mean weld diameters and calculated nugget diameters, the simulative results are in good accordance to the measured results. Thus, the accuracy of the FE-model is acceptable.

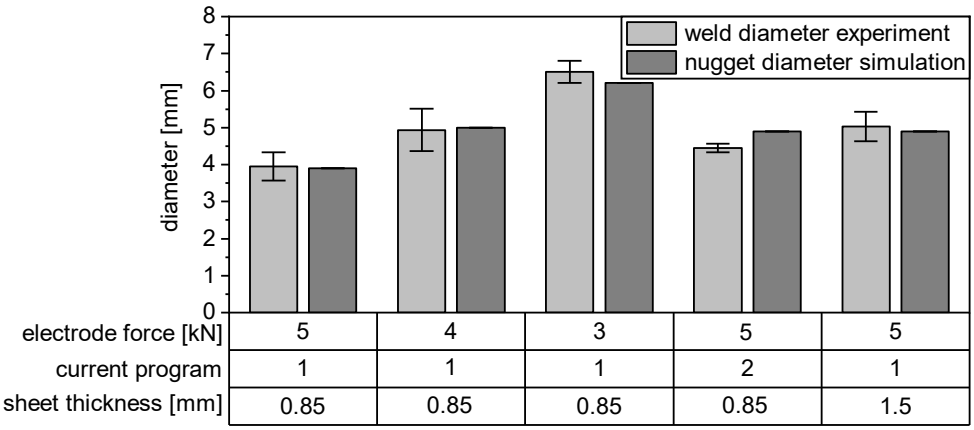

Fig. 16 Comparison of measured weld diameter and simulated nugget diameter

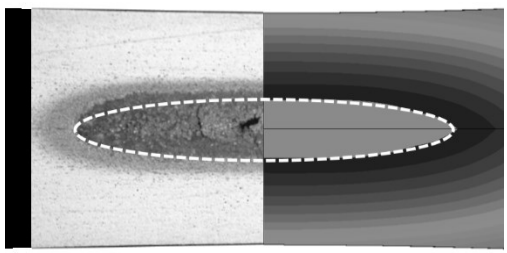

Fig. 17 Comparison of simulated and measured nugget geometry with electrode force 5 kN, current program 1 and sheet thickness 1.5 mm

Fig. 17 visualizes measured and calculated nugget geometry for electrode force of 5 kN, current program 1 and sheet thickness 1.5 mm. The isothermals are used to determine the geometry of the nugget by reaching melting temperature. Both, experimental and calculated nugget diameter are about 4.9 mm. Fig. 17 indicates that the experimental nugget penetration is higher to the direction of the anode-side electrode, which is located at the top. This phenomenon can be explained by Peltier effect, which is not considered in the numerical simulation. Though, the nugget thicknesses are comparable. Thus, the predicted nugget is matching well with the physical nugget profile, which indicates that the FE-model has a good accuracy.

SUMMARY AND CONCLUSION

In this article, the resistance spot welding process of aluminum, which is dominated by Joule heating at faying surface, has been investigated. The main focus was to develop an approach for contact resistance, which has been proved feasible to model the behavior of contact resistance in the RSW process of aluminum alloy AA5182, which is frequently used in automotive body in white shop. For this purpose, an experimental setup was developed in order to analyze the behavior of the apparent contact resistances in RSW process. A coupled thermal-electrical-mechanical FE-model was successfully used to determine apparent contact resistances as well as the resulting nugget geometry of the experiments.

In the first step, FE-simulations with temperature-dependent elastoplastic material properties for the aluminum sheets were used to calibrate the contact resistance model using measured resistance curves with respect to temperature and pressure dependent effects. Therefore, currents and voltage differences were measured in experiments by variation of applied current, electrode force and sheet thickness. The contact resistance model was fitted to match with measured resistances and is valid for sheet-sheet interface and electrode-sheet interface. Afterwards, in order to determine the accuracy of the calibrated contact resistance model, the heat generated by Joule heating at electrode-sheet and sheet-sheet interface was analyzed. As result, the averaged deviation between calculated and mean measured Joule heating amounts 3% for faying interface and about 5% for electrode-sheet interface. Hence, the obtained results of FE-simulation with the contact resistance model are reproducing experiments with good accuracy.

Further, the presented thermal-electrical-mechanical FE-model was validated. Therefore, the measured experimental nugget dimensions were compared to calculated ones. As result, calculated nugget diameters are matching with experimental weld diameter with a small averaged deviation of 4%, which represents good accordance.

In summary, the presented contact resistance model can reproduce the behavior of the contact resistance in RSW of aluminum alloy AA5182 with the essential effects and interactions. Thus, the thermal-electrical-mechanical FE-simulations are in good accordance to the experimental results.

In future, higher electrode forces and currents should be investigated. Moreover, other surface conditions and their effects on contact resistance should be analyzed. Also, sensitivity studies of the temperature dependent material properties need to be examined.

REFERENCES

[1] D. H. PHILLIPS: '*Welding engineering. An introduction*', John Wiley & Sons Ltd., 2016.

[2] S. M. MANLADAN, F. YUSOF, S. RAMESH, M. FADZIL, Z. LUO and S. AO: 'A review on resistance spot welding of aluminum alloys', *The International Journal of Advanced Manufacturing Technology*, pp. 605–634, 2017.

[3] U. DILTHEY: '*Schweißtechnische Fertigungsverfahren 1. Schweiß- und Schneidtechnologien*', Springer-Verlag Berlin Heidelberg, Berlin Heidelberg, 3. edition, 2006.

[4] Ducker Worldwide: '*Aluminum Content in North American Light Vehicles 2016 to 2028*', 2017. Online available at: http://www.drivealuminum.org/wp-content/uploads/2017/10/Ducker-Public_FINAL.pdf, proved: 2018/06/18.
[5] S. DAS: 'Life Cycle Energy and Environmental Assessment of Aluminum-Intensive Vehicle Design', *SAE International Journal of Materials and Manufacturing 7(3)*, pp. 588–595, 2014.
[6] M. KIMCHI and D. H. PHILLIPS: '*Resistance spot welding. Fundamentals and applications for the automotive industry*', Morgan & Claypool Publishers, San Rafael, California, 2017.
[7] M. J. GREITMANN, O. VOLZ and H.-J. WINK: 'Untersuchungen zum Übergangswiderstand an blanken und beschichteten Stahlblechen', *Schweißen und Schneiden 56 Heft 1,* 2004.
[8] R. HOLM: '*Electric contacts. Theory and application*', Springer-Verlag, Berlin, New York, 4. completely rewritten edition, 1967.
[9] S. TIMSIT: '*Electrical contact resistance: properties of stationary interfaces*', Electrical Contacts - 1998. Proceedings of the Forty-Fourth IEEE Holm Conference on Electrical Contacts. Arlington, VA, USA, pp. 1–19, 1998.
[10] E. VINARICKY, K. H. SCHRÖDER and J. WEISER: '*Elektrische Kontakte, Werkstoffe und Anwendungen. Grundlagen, Technologien, Prüfverfahren*', Springer Vieweg, Berlin Heidelberg, 3. edition, 2016.
[11] M. Galler: '*Investigation of interfacial contact condition during resistance spot welding of automobile sheet steel*', Graz, Technische Universität GrazDissertation, 2011.
[12] J. KAARS, P. MAYR and K. KOPPE: 'Simple transition resistance model for spot welding simulation of aluminized AHSS', *Mathematical modelling of weld phenomena 11*, edited by C. Sommitsch, N. Enzinger and P. Mayr, Verlag der Technischen Universität Graz, pp. 685–702, 2016.
[13] P. Rogeon, P. Carre, J. Costa, G. Sibilia, G. Saindrenan: 'Characterization of electrical contact conditions in spot welding assemblies', *Journal of materials processing technology 195,* 2008.
[14] S. S. M. VOGLER: 'Electrical contact resistance under high loads and elevated temperatures', *Welding Journal 72 (6)*, 231s–238s, 1993.
[15] Q. Song, W. Zhang, N. Bay: 'An experimental study determines the electrical contact resistance in resistance welding', *Welding Journal 84,* 2005.
[16] S. S. BABU, M. L. SANTELLA, Z. FENG, B. W. RIEMER and J. W. COHRON: 'Empirical model of effects of pressure and temperature on electrical contact resistance of metals', *Science and Technology of Welding and Joining*, pp. 126–132, 2013.
[17] J. A. GREENWOOD: 'Constriction resistance and the real area of contact', *British Journal of Applied Physics 17*, pp. 1621–1632, 1966.
[18] J. A. GREENWOOD and J. B. P. WILLIAMSON: 'Contact of nominally flat surfaces', *Proceedings of the Royal Society of London, Series A, Mathematical and Physical Sciences Vol. 293, No. 1442*, pp. 300–319, 1966.
[19] W. ZHANG: '*Design and Implementation of Software for Resistance Welding Process Simulations*', SAE Technical Paper 2003-01-0978, 2003.
[20] V. L. POPOV: '*Kontaktmechanik und Reibung. Von der Nanotribologie bis zur Erdbebendynamik*', 3. edition, 2015.

[21] J. A. KHAN, L. XU, Y.-J. CHAO and K. BROACH: 'Numerical Simulation of Resistance Spot Welding Process', *Numerical Heat Transfer, Part A: Applications*, pp. 425–446, 2000.

[22] R. OSSENBRINK and V. MICHAILOV: 'Thermomechanical Numerical Simulation with the Maximum Temperature Austenisation Cooling Time Model (STAAZ)', *Mathematical modelling of weld phenomena 8*, edited by H. Cerjak, Verlag der Technischen Universität Graz, pp. 357–372, 2007.